Deconvoluting the Mechanism of Microwave Annealing of Block Copolymer Thin Films

Cong Jin,[†,‡] Jeffrey N. Murphy,[†,‡] Kenneth D. Harris,[†] and Jillian M. Buriak[†,‡,*]

[†]National Institute for Nanotechnology, 11421 Saskatchewan Drive, Edmonton, Alberta T6G 2M9, Canada, and [‡]Department of Chemistry, University of Alberta, 11227 Saskatchewan Drive NW, Edmonton, Alberta T6G 2G2, Canada

ABSTRACT The self-assembly of block copolymer (BCP) thin films is a versatile method for producing periodic nanoscale patterns with a variety of shapes. The key to attaining a desired pattern or structure is the annealing step undertaken to facilitate the reorganization of nanoscale phase-segregated domains of the BCP on a surface. Annealing BCPs on silicon substrates using a microwave oven has been shown to be very fast (seconds to minutes), both with and without contributions from solvent vapor. The mechanism of the microwave annealing process remains, however, unclear. This work endeavors to uncover the key steps that take place during microwave annealing, which enable the self-assembly process to proceed. Through the use of *in situ* temperature monitoring with a fiber optic temperature probe in direct contact with the sample, we have demonstrated that the silicon substrate on which the BCP film is cast is the dominant source of heating if the doping of the silicon wafer is sufficiently low. Surface temperatures as high as 240 °C are reached in under 1 min for lightly doped, high resistivity silicon wafers (n- or p-type). The influence of doping, sample size, and BCP composition was analyzed to rule out other possible mechanisms. *In situ* temperature monitoring of various polymer samples (PS, P2VP, PMMA, and the BCPs used here) showed that the polymers do not heat to any significant extent on their own with microwave irradiation of this frequency (2.45 GHz) and power (~600 W). It was demonstrated that BCP annealing can be effectively carried out in 60 s on non-microwave-responsive substrates, such as highly doped silicon, indium tin oxide (ITO)-coated glass, glass, and Kapton, by placing a piece of high resistivity silicon wafer in contact with the sample—in this configuration, the silicon wafer is termed the *heating element*. Annealing and self-assembly of polystyrene-*block*-poly(2-vinylpyridine) (PS-*b*-P2VP) and polystyrene-*block*-poly(methyl methacrylate) (PS-*b*-PMMA) BCPs into horizontal cylinder structures were shown to take place in under 1 min, using a silicon wafer heating element, in a household microwave oven. Defect densities were calculated and were shown to decrease with higher maximum obtained temperatures. Conflicting results in the literature regarding BCP annealing with microwave are explained in light of the results obtained in this study.

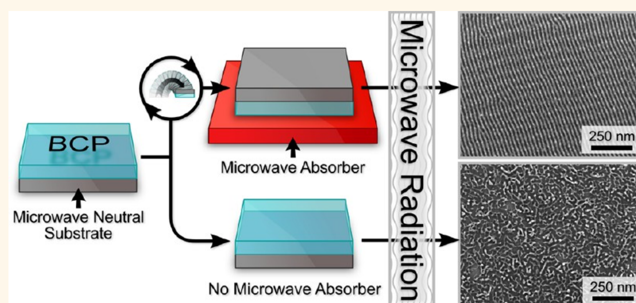

KEYWORDS: block copolymer · self-assembly · microwave irradiation · thermal annealing · defect density · thin film · patterning

Self-assembly of block copolymer (BCP) thin films has attracted a great deal of attention as a promising complementary technology to photolithography to enable high-resolution semiconductor chip manufacturing.[1−9] As a scalable and cost-effective bottom-up approach, the self-assembly of BCP films provides a possible route to sub-20 nm features, with little external intervention. Two decades of investigation of BCP self-assembly have shown it to be a versatile technology capable of creating a wide range of features, including cylinders,[10,11] lamellae,[12] hexagonally or rectangularly ordered dots,[13−15] and perforated lamellar structures.[16] When combined with intermittent topographic or chemical surface features,[17,18] an approach termed graphoepitaxy or directed self-assembly, self-assembled BCP patterns can present long-range order over many micrometers[14,18] and can be coerced to form more complex structures, such as circles,[10] bends,[19] junctions,[20] and jogs,[20] with low defect densities.[21−23] After using the BCP nanopattern as a template to form metal, metal oxide, or metal alloy nanostructures, BCP-templated nanomaterials have been harnessed as the basis for applications as phase change memory,[24−28] sensors,[29] transistors,[30] light-harvesting devices,[31] and catalytic nanostamps.[32−34] Owing to this promise, the latest International

* Address correspondence to jburiak@ualberta.ca.

Received for review February 14, 2014 and accepted March 21, 2014.

Published online March 21, 2014
10.1021/nn5009098

Published 2014 by the American Chemical Society

Technology Roadmap for Semiconductors (ITRS) describes BCP-based patterning technology as "a viable and competitive patterning option".[35]

To prepare well-ordered, self-assembled BCP thin films, annealing is a key step to facilitate the necessary reorganization of nanoscale phase-separated domains that generates the desired morphology. The most commonly used annealing methods are thermal annealing[22,36−46] and solvent annealing.[11,47−55] For thermal annealing, BCP thin films are heated to a temperature between the glass transition temperature (T_g) and order disorder transition temperature (ODT) for an extended period of time (on the order of days[36,56,57]) to enable plasticization of the polymer chains. In the case of solvent annealing, the BCP film is exposed to a vapor of a compatible solvent, where compatible indicates a solvent in which one or more blocks are soluble.[58] The solvent is absorbed by the BCP blocks, resulting in swelling of the polymer film. Solvent absorption brings about a decrease in the Flory−Huggins interaction parameter [$\chi_{eff} = \chi(1 - f)$, where f is the volume fraction of solvent in swollen BCP film], and owing to the shielding effect of the solvent, polymer chains then have increased mobility, resulting in lowering of the barrier to phase reorganization. Thermal annealing and solvent annealing are thus complementary approaches[59] since both lead to increased mobility of the BCP chains to assist the self-assembly process.

From a practical perspective, the time required for annealing is important for both commercial applications and research laboratory throughput. Faster is always more convenient. The 2007 ITRS roadmap specifically stated that the BCP annealing process needed to be complete in under 4 min;[60] by 2011, improvements in the time required for annealing were noted by the roadmap, and it stated that "a few minutes...represents a realistic time scale for potential processing applications".[35] As a result, there has been a determined effort to reduce the time required for annealing.[61−63] For instance, in 2010, Zhang and co-workers showed that polystyrene-*block*-poly(2-vinylpyridine) (PS-*b*-P2VP) and polystyrene-*block*-poly(methyl methacrylate) (PS-*b*-PMMA) films could assemble into aligned horizontal cylinders in 60−180 s with solvent-assisted microwave annealing.[21] In 2012, another solvothermal approach (on conventional hot plate) combined with graphoepitaxy successfully brought about self-assembly of line patterns from polystyrene-*block*-polydimethylsiloxane (PS-*b*-PDMS) in 5 min.[64] In 2013, when combined with graphoepitaxy, sequential solvent and thermal annealing was carried out with PS-*b*-PDMS to assemble a hexagonal dot pattern in 30 s.[65] Very recently, a non-graphoepitaxial rapid thermal processing approach to 250 °C was shown to be applicable to PS-*b*-PMMA and resulted in fingerprint line patterns in a minimum of 60 s.[16] There remain, however, questions as to the applicability of thermal and solvent annealing processing in an integrated circuit (IC) manufacturing environment; at present, a solvent annealing step has not yet been developed within the context of semiconductor processing, and therefore, thermal annealing may be more readily adopted.[66]

Microwave-based heating is a subtly different approach toward thermal annealing that has been only superficially explored for BCP annealing. Given its simplicity and speed, microwave annealing merits continued investigation.[35] Microwave heating is well-established in industrial, academic, and domestic settings as a rapid, non-classical heating technique.[67−69] It was first used primarily in the food industry in the 1960s, but thereafter, its use rapidly expanded to other large-scale manufacturing, including the curing of rubber and wood products, ceramics, and semiconductors.[70] Microwave heating is commonly used in academic laboratory settings since the rate of many reactions can be dramatically increased, often leading to higher yields and product purities.[68,71,72] Since microwave irradiation can heat and even melt silicon wafers,[73] the typical substrate used for self-assembly of BCP thin films, our group proposed in 2010 that a research grade microwave oven could be used to anneal BCP thin films on silicon wafers.[21] BCP thin films on silicon wafer shards of known resistivities were sealed in a glass vial, with or without a solvent, and heated in a research grade microwave oven. Analysis of the resulting BCP structures clearly demonstrated that this microwave-assisted solvothermal annealing process dramatically decreased the observed defect density and reduced the anneal time to only minutes (and, in many cases, to 1 min).[21] It was demonstrated soon afterward that an inexpensive domestic microwave oven could also be used to anneal the BCP films, which opened up the annealing technique to any lab.[74] This initial work was followed up by Morris and coworkers who demonstrated that microwave annealing could be applied to fabricate cylinder and perforated lamellar patterns on the order of minutes, also in a research grade microwave reactor, both with and without solvent.[75,76]

The mechanism of the microwave annealing process is, at present, disputed, and there are conflicting results that complicate interpretation. The role of the silicon wafer as a source of thermal heating has been questioned, with one group pointing to links between silicon wafer resistivity and annealing rates for the BCP self-assembled nanopatterns (and also to wafer heating evidenced by wax melting experiments),[21,74] and another group categorically stating that the silicon wafer heating cannot account for the observed annealing of BCPs.[74,76] Further convoluting matters, two papers showed opposing trends with respect to wafer resistivity and BCP annealing rates and defect

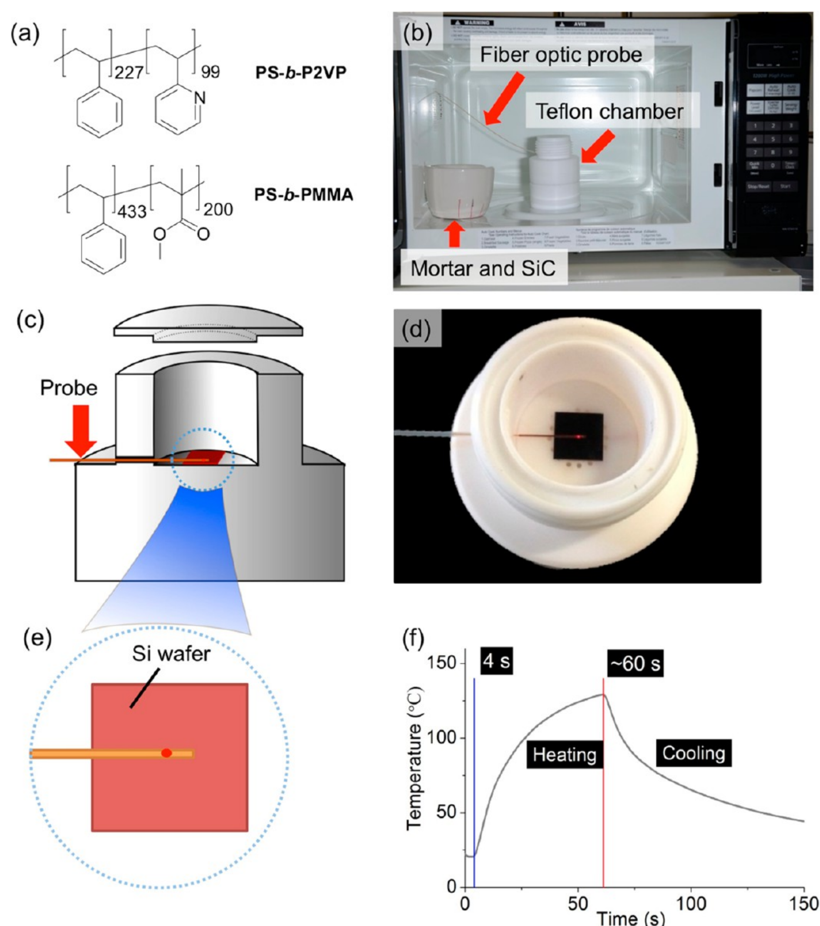

Figure 1. (a) Structures of the two block copolymers used in this work. (b) Photograph of the microwave annealing apparatus. (c) Cross-sectional drawing of the Teflon chamber with fiber optic probe and silicon wafer. (d) Photograph of the Teflon chamber with fiber optic probe and silicon wafer inside. (e) Scheme of silicon wafer with a fiber optic probe for temperature measurement. The red dot on the probe is fluorescent ceramic material encased in 0.6 mm diameter polyimide sphere. (f) Temperature profile of a 1 × 1 cm^2 silicon wafer shard (p-type, 525 ± 25 μm thickness, 6.2 $\Omega \cdot$cm) heated in a domestic microwave oven for ~60 s.

densities.[21,74] In all of the prior work, the *in situ* temperature of the substrate and polymer was not measured because the research grade microwave ovens rely upon an infrared thermometer that measures the temperature of the glass vial in which the samples are contained, rather than directly measuring the sample temperature itself. There is no reason to assume that the temperature of the glass vial would be the same as a shard of a silicon wafer contained within, given the non-equilibrium, non-isothermal nature of the system, low thermal conductivity of glass, and the poor contact between the shard and the vial.[21,75,76] The domestic (kitchen) microwave ovens are similarly hampered with respect to *in situ* temperature monitoring. BCP annealing is tantalizing in its rapidity and simplicity, but in order to effectively utilize the technique, optimize it, and generalize to different BCPs and substrates, the fundamentals of the mechanism of microwave annealing need to be detailed, deconvoluted, and fully understood. In this work, we use microwave-compatible fiber optic probes to directly measure the temperatures of all the components within the microwave oven in real time. A fluorescence-based fiber optic probe was selected on account of the small heat capacity (0.6 mm diameter with a polyimide tip), microwave compatibility, and fast response time. All materials were analyzed independently, and together, and the results compared. We confirm the source of heating by decoupling the "heating element" (those materials that heat up with microwave irradiation) from the substrate, and we show that an independent microwave-susceptible heating element can be used for an arbitrary composition of BCP thin film and underlying substrate.

RESULTS AND DISCUSSION

BCPs are composed of two or more dissimilar homopolymer chains (blocks) connected by covalent bonds, and under specific conditions, BCP films undergo nanoscale phase segregation. Two representative diblock copolymers, having two blocks in one polymer chain, were used in this work: PS-*b*-P2VP (23.6k-*b*-10.4k, PDI = 1.04) and PS-*b*-PMMA (45k-*b*-20k, PDI = 1.07) (structures shown in Figure 1a). BCP thin films with

TABLE 1. Resistivity and Dopant Composition of Silicon Wafer Pieces Used for the Microwave Heating Experiments

ρ/Ω·cm	11.9	10.5	8.4	6.4	6.4	2.4	0.6	0.016	0.0041
type	p	n	p	p	n	p	p	p	p
dopant	B	P	B	B	P	B	B	B	B

thicknesses of ~40 nm were spin-cast on a silicon surface, unless stated otherwise, and placed in a Teflon chamber (Figure 1c,d). To measure and record the temperature during annealing, a microwave-compatible fiber optic probe was fed through a small hole in the Teflon chamber to make direct contact with the sample, as shown in Figures 1c–e. Additional photographs detailing the setup are shown in the Supporting Information (Figure S1). A typical heating profile for a lightly doped silicon wafer shard is shown in Figure 1f.

That silicon wafers can absorb microwave radiation and generate heat has been known for many decades. In the 1980s, a specially designed microwave device (given the name "microwave drill") was designed to melt silicon wafers in a spatially defined, localized fashion.[73] This work, and others, built upon the established observation that high resistivity silicon wafers heat more rapidly with microwave irradiation (frequencies of 2.45,[74] 2.856,[73] and 28 GHz[77]), while low resistivity wafers are slow to heat up.[74,77] For BCP annealing, the relationship between silicon wafer resistivity and geometry and the heating profiles during irradiation under the conditions applied for BCP annealing remain unknown. To examine the influence of the resistivity and dopant type over the temperature profile of silicon, wafers of similar thicknesses (525 ± 25 μm) but of different resistivities and dopant types (Table 1) were cut into 1.5 × 1.5 cm^2 pieces. Each silicon piece was placed in a Teflon chamber, and the fiber optic probe was placed in direct physical contact with the silicon for *in situ* monitoring (Figure 1c–e). When the wafer temperature reached 200 ± 3 °C, or the annealing time reached 60 s, the microwave oven was turned off manually. Temperature profiles for these silicon pieces are plotted in Figure 2a. The temperature of the silicon wafers did not change in the first 4 s, due to a 4 s lag required to activate the cavity magnetron after the microwave oven was turned on (Figure 1f). After 4 s, silicon pieces would undergo an increase in temperature until the microwave oven was turned off manually (Figure 1f).

As summarized in Figure 2a, high resistivity silicon pieces (ρ > 0.6 Ω·cm) could reach 200 °C within 30 s of microwave irradiation, and with this resistivity (or higher), the silicon wafer pieces presented very similar heating curves. Low resistivity wafers ($\rho \leq$ 0.6 Ω·cm) could not reach 200 °C within 60 s of microwave irradiation. The initial heating rates of each silicon piece were calculated from the first 7 s of heating (t = 4–11 s on the temperature profile plot of Figure 2a), and the results are displayed graphically in Figure 2b. As can be seen from Figure 2, the following trend is visible—the heating rate increases with greater resistivity and does not appear to be dependent upon the type of doping (n- and p-type dopants produce similar results).

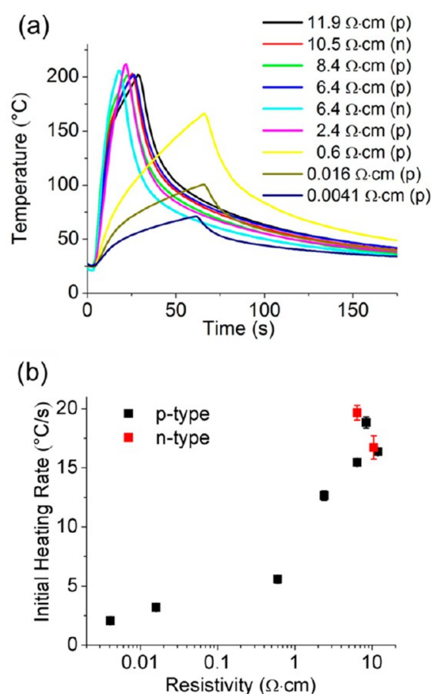

Figure 2. (a) Temperature profiles of 1.5 × 1.5 cm^2 silicon pieces of different resistivities and doping types during microwave irradiation. (b) Plots of initial heating rate (obtained from 4 to 11 s on each heating profile *versus* resistivity. Error bars (representing ± one standard deviation) are present on all points in (b) but are mostly invisible (see Table S1).

While not seemingly of interest, the relationship between wafer size and heating profile must also be understood, particularly with an eye on future scale-up. A 4 in. silicon wafer (p-type, 525 ± 25 μm thickness) with a resistivity of 6.2 Ω·cm was cut into 2.5 × 2.5, 2 × 2, 1.5 × 1.5, 1 × 1, and 0.5 × 0.5 cm^2 square pieces. When the temperature of the wafer reached about 200 ± 3 °C or the annealing time reached 60 s, the microwave oven was turned off manually. The temperature of the silicon wafer piece was monitored until the temperature dropped to around 40 °C. Temperature profiles of these silicon pieces are plotted in Figure 3a. The largest piece, the 2.5 × 2.5 cm^2 silicon shard, heated the fastest, reaching 200 °C at the 11 s mark. The 2 × 2 cm^2 sample was similar to the largest piece, reaching 200 °C at the 13 s mark. As the pieces became smaller, the time required to reach 200 °C increased, with the 1.5 × 1.5 cm^2 shard requiring 26 s. The smaller silicon pieces, 1 × 1 and 0.5 × 0.5 cm^2, could not reach 200 °C within 60 s. The initial heating rates of each silicon piece were calculated using the temperature profiles from 4 to 11 s, and they are

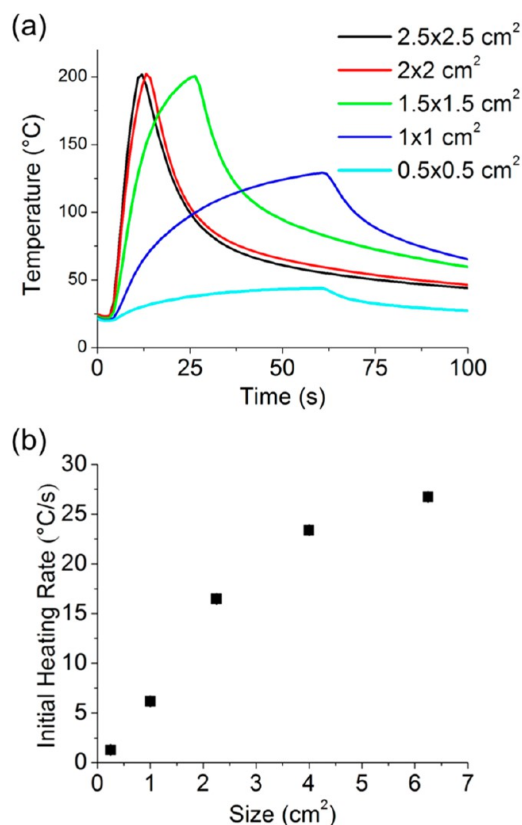

Figure 3. (a) Temperature profiles for different sizes of silicon pieces cut from one silicon wafer (p-type, 525 ± 25 μm thickness, 6.2 Ω·cm). (b) Initial heating rate of silicon pieces *versus* area, obtained from 4 to 11 s on each heating profile. Error bars (representing ± one standard deviation) are present on all points in (b) but are mostly invisible (see Table S2).

plotted in Figure 3b. These data suggest a linear increase in the initial heating rate as sample size increases from 0.5 × 0.5 to 1.5 × 1.5 cm^2, but that the linearity does not continue above this size (the rate of temperature increase appears to drop with larger sizes). This observation may be a result of overlap between the sample and a "hotspot" in the microwave, which occurs at half the wavelength, or 6.1 cm, as sample position was consistent, but not optimized for maximum heating rate; alternatively, spatial variations of heat flow into the Teflon holder might account for this observation. Samples larger than 2.5 × 2.5 cm^2 are not reported here because they exceed the size of the Teflon chamber.

It has been postulated that the BCP itself could heat up with microwave irradiation and could therefore act as the heat source that induces nanoscale phase reorganization.[76] To understand whether either BCP block absorbs microwave radiation and induces local heating independent of the silicon substrate, five thick films (PS, P2VP, PMMA) and two mixtures (PS+P2VP and PS+PMMA) were drop-cast onto low resistivity (p-type, 525 ± 25 μm thickness, 0.0044 Ω·cm, 1 × 1 cm^2) silicon substrates, as shown in Table S3. The weight ratios of homopolymers in the two blend films are close to the weight ratio in PS-*b*-P2VP and PS-*b*-PMMA used in this work. These silicon wafers had already been shown to maintain a relatively static temperature under these conditions. Each homopolymer film was placed in the center of the Teflon chamber in contact with the fiber optic temperature probe and was irradiated in the microwave oven for around 60 s. The samples coated with homopolymers each heat up to about 32 °C with ~60 s of applied microwave power, which is far below their T_g (about 100 °C) and the temperature expected for successful annealing. Temperature profiles for each homopolymer on silicon, as well as control profiles for the silicon substrate without polymer and the fiber optic temperature probe without either silicon or polymer are plotted in Figure S2. Because the homopolymers are poor microwave absorbers, as is consistent with the low dielectric loss tangents for each material (PS, PMMA, P2VP, and also PDMS, provided in Table S4),[78] they alone cannot absorb sufficient microwave energy to surpass T_g. The source of the heating must arise from the silicon substrate if it has a sufficiently high resistivity.

Since it was determined that the silicon substrate was the source of heating upon microwave irradiation, separate materials were used as microwave *heating elements* and BCP *substrates*, as shown schematically in Figure S3. The heating element is thus decoupled from the BCP thin film on the substrate and allows for microwave annealing on any substrate material, including those that are irresponsive to microwaves. To demonstrate this concept, a 1.5 × 1.5 cm^2 silicon wafer (p-type, ⟨100⟩, 525 ± 25 μm thickness, 8.4 Ω·cm) was chosen as the heating element. Microwave-irresponsive materials, such as low resistivity silicon wafers (0.0044 Ω·cm), ITO-coated glass, glass, and Kapton were used as substrates and spin-coated with ~1% w/w toluene solutions of PS-*b*-P2VP and PS-*b*-PMMA to form thin films about 40 nm in thickness, as measured by ellipsometry. The BCP-coated substrates were then placed on the 1.5 × 1.5 cm^2 silicon heating element with the BCP thin film between them, forming a sandwich structure (see Figure S3). The fiber optic probe was installed in the Teflon chamber and placed in contact with the silicon heating element. During microwave annealing, the microwave oven was again turned off manually once a certain predefined temperature was obtained. For BCP films on silicon, the temperatures at which the microwave heating was shut off ranged from 160 to 240 °C, and for BCP films on ITO-coated glass, glass, and Kapton, heating was terminated at 240 °C. As control experiments, substrates with the same BCP films but no heating element were microwave annealed for 1 min. In those experiments where PS-*b*-P2VP was employed, the annealed BCP template was converted to Pt nanopatterns to improve contrast for SEM imaging.[10,79,80] Annealed PS-*b*-PMMA samples required only a brief oxygen plasma treatment to

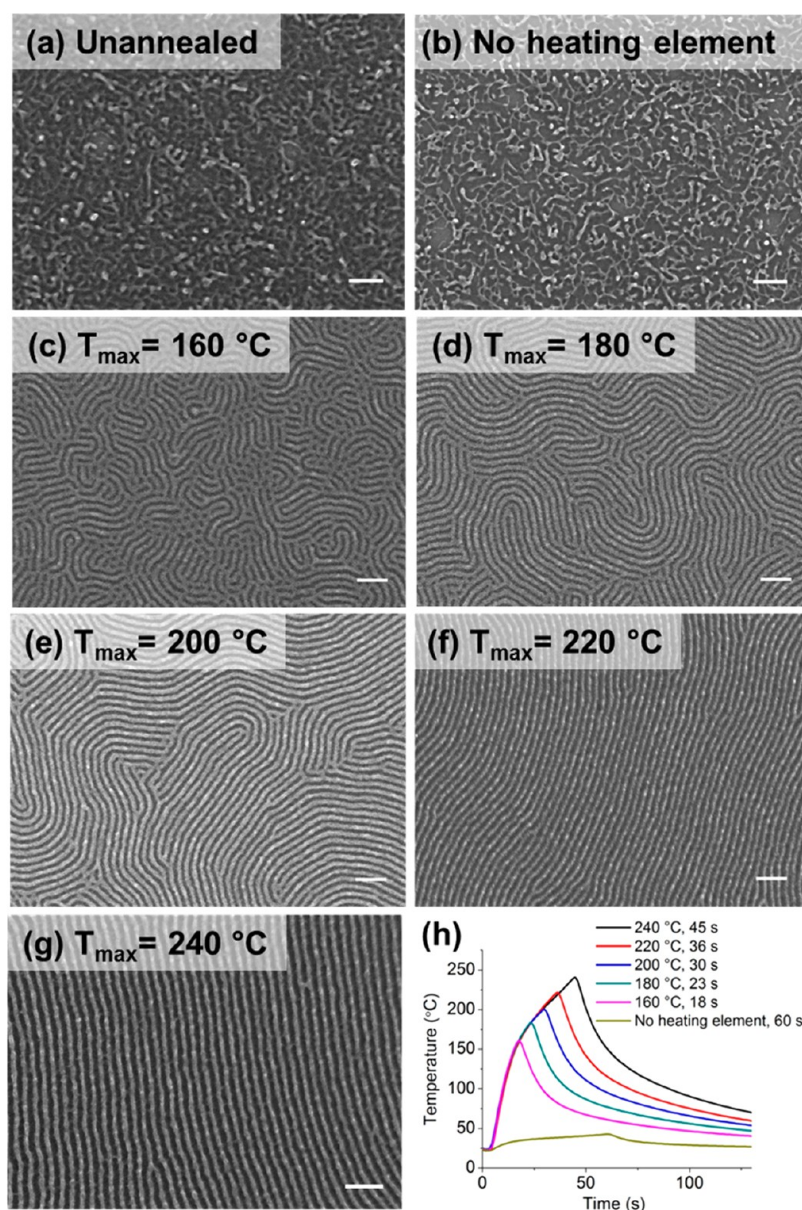

Figure 4. Influence of the temperature of the heating element on the morphology of the PS-*b*-P2VP thin film. (a) SEM image of Pt features produced using an unannealed PS-*b*-P2VP thin film for comparison. (b) SEM image of Pt features produced from PS-*b*-P2VP thin films heated in microwave oven for 60 s without a heating element. (c−g) SEM images of Pt features produced from PS-*b*-P2VP thin films that had been annealed to 160, 180, 200, 220, and 240 °C, respectively. (h) Temperature profiles for each of these samples. All scale bars are 100 nm.

remove part of the PMMA block to aid visualization by SEM.[14,81]

Figures 4 and 5 show the SEM images of Pt nanopatterns prepared from PS-*b*-P2VP and PS-*b*-PMMA self-assembled thin films, respectively, annealed at different temperatures. Temperature profiles corresponding to the images in Figures 4a−g and 5a−g are also provided in Figures 4h and 5h. Silicon wafers that heat to no appreciable extent upon microwave irradiation (p-type, 1 × 1 cm^2, ⟨100⟩, 525 ± 25 μm thickness, 0.0044 $\Omega\cdot$cm) were used as substrates for PS-*b*-P2VP and PS-*b*-PMMA thin films (∼40 nm). As can be seen in Figure 4b, without the heating element, the BCP is essentially unchanged after 60 s of microwave irradiation as compared to the unannealed sample in Figure 4a because the temperature did not exceed 50 °C (Figure 4h). With the heating element in contact with the microwave-irresponsive heavily doped silicon substrate, increased ordering of the horizontal cylinders can be seen upon increasing the maximum attained temperature from 160 to 240 °C (Figure 4c−e). Similar results are observed for the PS-*b*-PMMA films (Figure 5). The presence of a heating element results in formation of better ordered horizontal cylinder patterns when the temperature is increased from 160 to 240 °C (Figure 5g).

The defect densities of the PS-*b*-P2VP and PS-*b*-PMMS samples shown in Figures 4 and 5 were calculated and plotted in Figure 6. The plots show that the

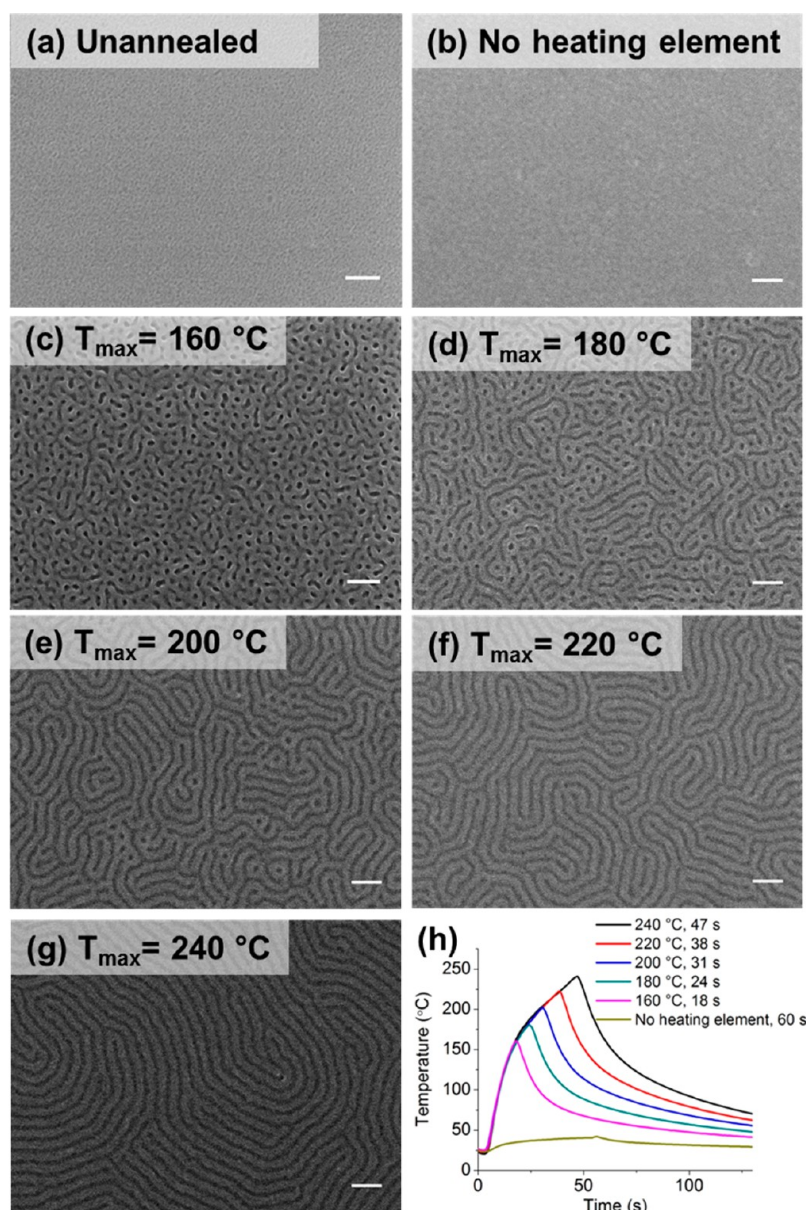

Figure 5. Influence of annealing temperature with and without the heating element on the morphology of the PS-*b*-PMMA thin film. (a) SEM image of unannealed PS-*b*-PMMA thin film. (b) SEM image of PS-*b*-PMMA thin film heated in microwave oven for 60 s without heater a heating element. (c−g) SEM images of PS-*b*-PMMA thin films annealed to 160, 180, 200, 220, and 240 °C, respectively. (h) Temperature profiles for each of these samples. All scale bars are 100 nm.

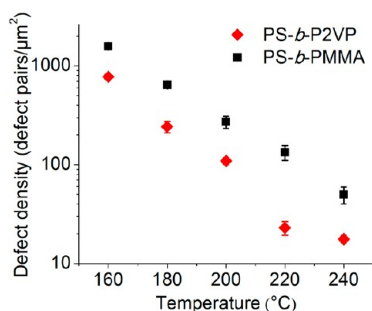

Figure 6. Plot of defect density *versus* peak annealing temperature for PS-*b*-P2VP and PS-*b*-PMMA thin films.

defect density decreases exponentially with maximum annealing temperature. For PS-*b*-P2VP, an ordered pattern with a defect density of 17.6 ± 1.5 pairs/μm^2 could be obtained by reaching an annealing temperature of 240 °C, which corresponds to 41 s of microwave irradiation. However, the defect densities of PS-*b*-PMMA samples could only be decreased to 49.8 ± 10.0 pairs/μm^2 when annealed to 240 °C in 43 s. These values exceed the level suggested by the ITRS for commercialization but are in line with others' results obtained without control of orientation (*i.e.*, graphoepitaxy) that have been reported in the literature.[16,21] The annealing process, at this point, is entirely unoptimized as it is performed on a neutral surface without graphoepitaxy, and modifications, such as tuning of surface properties, would be expected to reduce defect

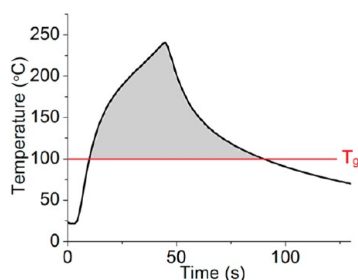

Figure 7. Black line: heating profile for a PS-*b*-P2VP sample on a low resistivity silicon substrate (0.0044 Ω·cm). Red line: T_g of PS-*b*-P2VP. Gray area: time above T_g experienced by the PS-*b*-P2VP sample.

TABLE 2. Time Spent Above T_g for PS-*b*-P2VP and PS-*b*-PMMA Thin Films on Heavily Doped Silicon Wafer Shards Annealed to Different Temperatures

T_{max}/°C		240	220	200	180	160
time (T_g to T_g)/s	PS-*b*-P2VP	79.9	60.3	46.4	31.2	18.9
	PS-*b*-PMMA	87.2	71.1	53.9	35.6	20.7

densities further.[21−23] In addition, more sophisticated heating profiles could be designed to maintain the temperature above T_g or to carry out multiple rapid anneals to "exercise out" defects through programmed heating and cooling cycles. One variable that was not specifically controlled is the length of time the BCP films are held above the T_g, as represented by Figure 7. Time above T_g refers to the length of time each BCP thin film was above its T_g, as tabulated in Table 2. As expected, the time at and above the T_g increases with an increase in the maximum annealing temperature. Controlling for the length of time the sample spends above T_g is an important variable that is the subject of future work.

Because the heating element is decoupled from the BCP thin film (on its own substrate), the use of the heating element should enable microwave annealing on non-silicon substrates, such as ITO-coated glass, glass, and Kapton. The temperature profiles for these three substrates are shown in Figures 8 and 9 for PS-*b*-P2VP and PS-*b*-PMMA, respectively. As seen in Figures 10 and 11, BCP annealing and self-assembly is successful on ITO-coated glass, glass, and Kapton when using the heating element configuration because the temperature rapidly exceeds the polymer T_g. The ITO-coated glass, glass, and Kapton were cut into 1 × 1 cm^2 in size, and PS-*b*-P2VP and PS-*b*-PMMA thin films (∼40 nm) were spin-coated on these clean substrates in the same fashion as described earlier for silicon surfaces. The temperature of PS-*b*-P2VP thin films on ITO-coated glass reached 45 °C after ∼60 s of microwave irradiation without the heating element, while the glass and Kapton showed no apparent change in temperature (dashed curves in Figures 8 and 9).

The BCP thin film samples were then placed on the same heating element as described previously

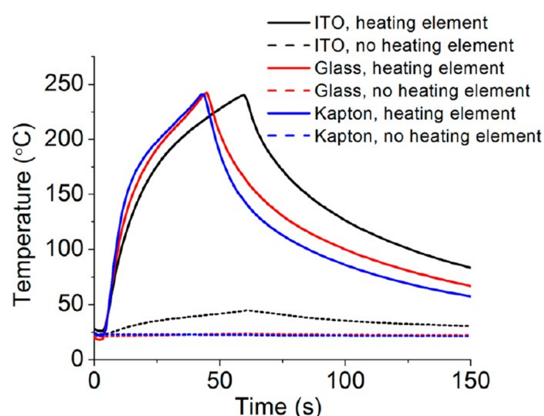

Figure 8. Temperature profiles of PS-*b*-P2VP thin films coated on ITO-coated glass, glass, and Kapton, annealed with and without a heating element.

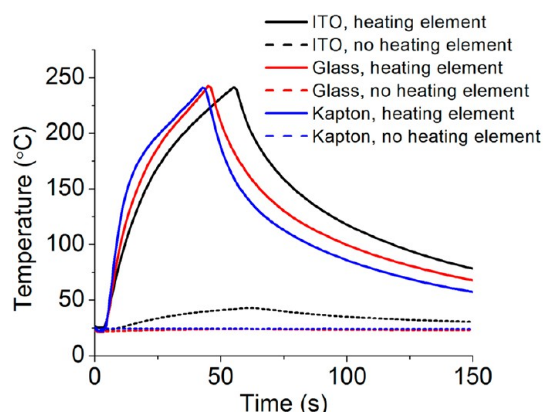

Figure 9. Temperature profiles of PS-*b*-PMMA thin films coated on ITO-coated glass, glass, and Kapton, annealed with and without a heating element.

(1.5 × 1.5 cm^2, p-type, ⟨100⟩, 525 ± 25 μm thickness, 8.4 Ω·cm). Three PS-*b*-P2VP samples were annealed to 240 °C with a heating element, and the results are shown in Figure 10a−c. The corresponding temperature profiles are shown in Figure 8. It takes ∼20 s longer for PS-*b*-P2VP thin film on ITO-coated glass to reach 240 °C, compared to those of PS-*b*-P2VP films on glass and Kapton (45 s). The time above T_g for the PS-*b*-P2VP thin film coated on ITO-coated glass is longer than that of films on glass and Kapton (Table 3). Without the heating element, the appearance of BCP films on ITO-coated glass, glass, and Kapton (Figure 10d−f) are not changed after 60 s of microwave irradiation, compared to unannealed samples (Figure 10g−i).

Similar results were obtained for PS-*b*-PMMA thin film samples as shown in Figure 11; the corresponding temperature profiles are shown in Figure 9. Samples were annealed to 240 °C with a heating element, and images of the annealed film are shown in Figure 11a−c. About 60 s were required for PS-*b*-PMMA thin films on ITO-coated glass to reach 240 °C, which is about 10 s longer than that of a PS-*b*-PMMA thin film on glass or Kapton (about 45 s). The time above T_g for the

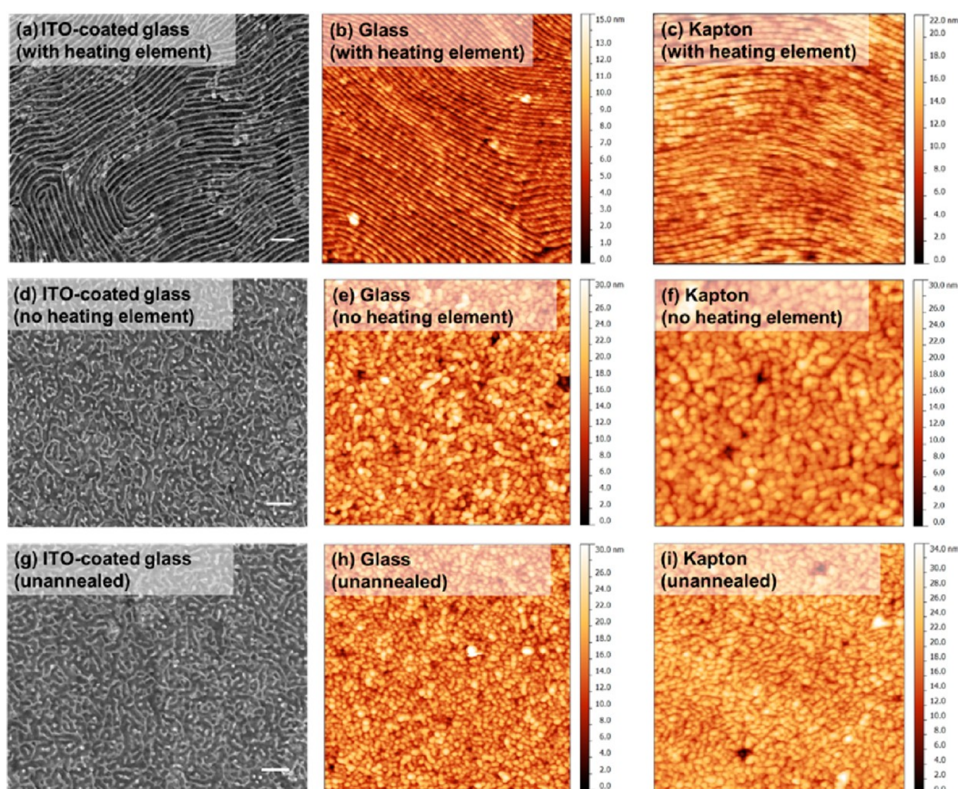

Figure 10. SEM images and AFM images of Pt features prepared from PS-*b*-P2VP thin films annealed with and without a heating element and unannealed PS-*b*-P2VP thin films on ITO-coated glass, glass, and Kapton. All scale bars are 100 nm. The sizes of AFM images are all $1 \times 1\ \mu m^2$.

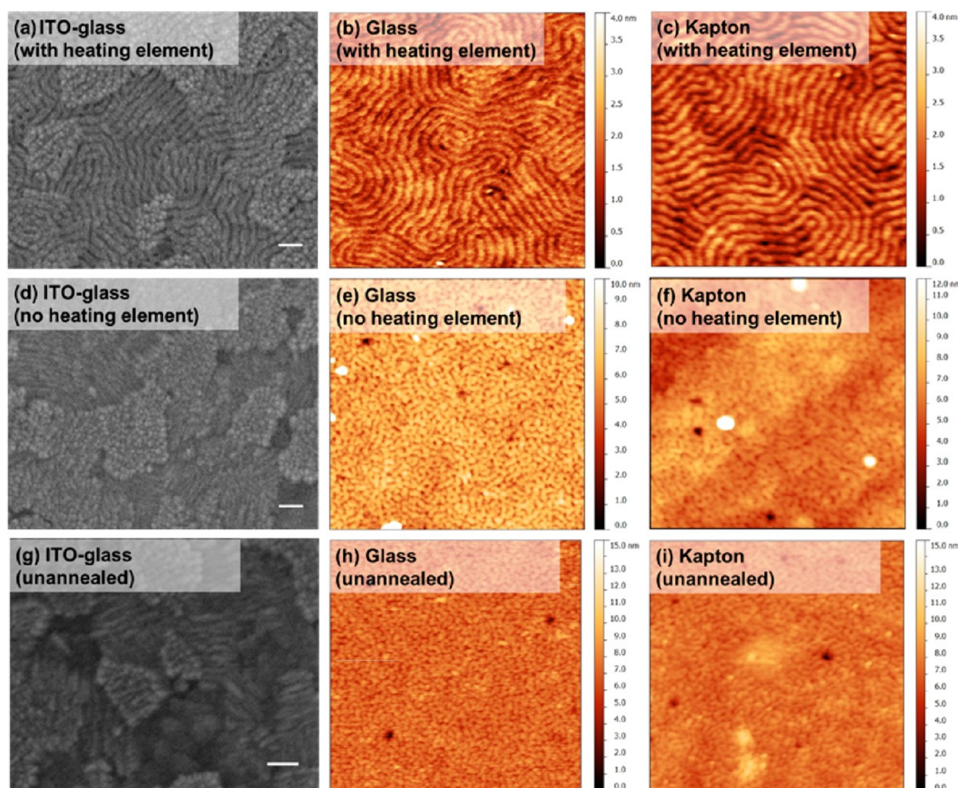

Figure 11. SEM images and AFM images of PS-*b*-PMMA thin films annealed with a heating element, without a heating element, and unannealed PS-*b*-PMMA thin films on ITO-coated glass, glass, and Kapton. All scale bars are 100 nm. The sizes of AFM images are all $1 \times 1\ \mu m^2$.

TABLE 3. Time Above T_g for PS-*b*-P2VP and PS-*b*-PMMA Thin Films on ITO-Coated Glass, Glass, and Kapton Annealed to 240 °C

substrate		ITO-coated glass	glass	Kapton
time (T_g to T_g)/s	PS-*b*-P2VP	115.1	90.4	76.8
	PS-*b*-PMMA	113.1	95.7	81.6

PS-*b*-PMMA thin film on ITO-coated glass was also longer than that on glass or Kapton (see Table 3). Small regions of a perforated lamellar structure were observed with a PS-*b*-PMMA thin film on ITO-coated glass (Figure S8), due to its high surface roughness (Figure S7).

To summarize, BCP thin films can be rapidly annealed using microwave irradiation, and this annealing effect appears to be due to heating of a microwave-responsive material with which the sample is in contact. The proposal that a non-thermal microwave effect, possibly related to changes in local electromagnetic fields during the anneal,[69] is responsible for the annealing effect is implausible, as all available data point to rapid heating of the substrate/heating element under the influence of microwave irradiation as a driving mechanism. In the first report of BCP annealing by our group (2010), it was concluded that defect densities of the resulting BCP samples were lower for low resistivity silicon substrates,[21] which is the opposite of what we observed here. The second report in 2011 showed the opposite effect: high resistivity, faster-heating silicon led to better annealing in a domestic microwave oven, which is consistent with what we observe here.[74] In this 2011 report, *in situ* melting of paraffin wax experiments demonstrated the relationship between substrate resistivity and thermal output, in some cases even led to the vaporization of the wax.[74] Finally, there are reports by others that have suggested that heating contributions from the substrate are insignificant and do not contribute to the annealing process.[75,76] The discrepancy of results arises, we believe, from the following. In our 2010 paper, sealed glass vessels were used in a research grade microwave reactor, and the programmed temperature profile had an unknown relationship with the temperature of the wafer contained within.[21] In a research grade microwave reactor, the temperature is measured at the external surface of the glass vial using infrared thermometry, and therefore, it does not necessarily reflect the temperature of objects inside the vial. The research grade reactor also uses a temperature-feedback loop to control the microwave power output. The controller decreases microwave power as the surface temperature of the vial, which in the 2011 paper was in direct thermal contact with the solvent, approaches its target.[74] It must be remembered that the presence of solvent leads to defect densities that are at least one and, in many cases, several orders of magnitude lower than without solvent.[21,74] When samples are exposed to solvent, the annealing is termed solvothermal and is a more complex system than simple thermal annealing due to accompanied swelling of the BCP film. In the 2011 microwave paper, a domestic kitchen microwave was used, and the samples were "sealed" in a Teflon chamber with warm THF.[74] Due to high vapor pressure, the BCP film (on a lightly doped silicon substrate: 10−20 Ω·cm) most likely underwent immediate swelling with solvent after it was placed in the chamber, but before microwave heating could be commenced manually. We conclude that this solvothermal approach is, in fact, a two-stage solvent and thermal annealing process that begins with solvent annealing and is followed by solvothermal annealing. While it needs to be determined, the heating of a BCP film swollen with solvent to $T > 200$ °C may completely expel the low-boiling-point solvent, at which point the annealing transitions to a predominately thermal process. Parallels may be made to the sequential solvent and thermal annealing process recently described by Kim and co-workers[59] and by Gotrik and Ross.[65]

CONCLUSION

The mechanism of microwave-driven annealing of BCPs to enable self-assembly into nanoscale patterns on surfaces has been elucidated. In this work, it was demonstrated through use of *in situ* temperature probes in direct contact with the sample surface that the underlying silicon substrate is the key to the rapid heating observed. Lightly doped silicon wafers can reach temperatures in excess of 200 °C in seconds, whereas the BCPs themselves do not heat to any significant extent. The critical role of the silicon wafer was proven by carrying out microwave-induced BCP annealing on non-microwave-responsive materials such as glass and Kapton plastic; in this case, a separate piece of lightly doped silicon that does rapidly heat with microwave irradiation, termed the heating element, can be used to heat the BCP film and bring about annealing. Because the heating element can be decoupled from the substrate on which the BCP film self-assembly takes place, microwave annealing can thus be considered as a general approach and may permit spatially defined local heating through the use of a patterned heating element.

METHODS

Materials. PS-*b*-P2VP (23.6k-*b*-10.4k), PS-*b*-PMMA (45k-*b*-20k), and P2VP (154k) were purchased from Polymer Source Inc. Sodium tetrachloroplatinate(II) hydrate, $Na_2PtCl_4 \cdot xH_2O$, was obtained from Strem Chemicals. Concentrated aqueous HCl, concentrated H_2SO_4, and acetone were obtained from Caledon Laboratories Ltd. H_2O_2, dichloromethane, SiC powder, PS (192k), and PMMA (120k) were obtained from Sigma-Aldrich. Toluene

and isopropyl alcohol were obtained from Fisher Scientific. Silicon wafers (thickness: 525 ± 25 μm) were obtained from University Wafer and WRS Materials; glass substrates were ordered from Fisher Scientific (Catalog No.: 12−550-A3, 25 × 75 × 1.0 mm), and ITO-coated glass (sheet resistance: 8−12 Ω/□) substrates were purchased from Delta Technologies Ltd. Kapton film (PIT5N/12.7) was purchased from Caplinq.

Cutting. Silicon wafers were cut to the desired size with a dicing saw (Disco DAD 321). For dicing glass or ITO-coated glass, a Diamond Touch cutting saw was used.

Substrate Cleaning Procedure. Silicon and glass substrates were cleaned using piranha solution: samples were immersed into a 3:1 (v/v) mixture of concentrated sulfuric acid and 30% aqueous hydrogen peroxide for 15 min, rinsed with ultrapure (18.2 MΩ·cm) water, and dried with a nitrogen stream. For ITO-coated glass pieces, successive 15 min ultrasonication steps in dichloromethane, ultrapure water, and isopropyl alcohol were applied, and then the substrates were dried with a nitrogen stream. Kapton substrates were rinsed in toluene and acetone and then dried with a nitrogen stream.

Block Copolymer Thin Film Preparation. Block copolymer powder was dissolved in toluene to make ∼1% w/w solutions. These solutions were then stirred for at least 30 min, and then 15 μL volumes were dropped onto clean substrates and spin-coated at 3000 rpm for 15 s under an argon environment. The thicknesses of block copolymer thin films as determined by ellipsometry were generally ∼40 nm.

Microwave Annealing Procedure. Where not otherwise specified, a general process was employed: Microwave annealing was performed in modified Panasonic microwave ovens (model number NNST651B, purchased from Walmart), using inverter technology to provide constant power, up to 1200 W, varying linearly with power setting, rather than cycled pulses. A mortar with about 100 g SiC powder (200−450 mesh) was placed in the right side of microwave oven to absorb excess microwave radiation and prevent damage to the microwave. A fluorescence-based fiber optic temperature probe (model number PRB-G40-2.0M-ST-C with polyimide tip and calibration to 250 °C and accuracy of ±0.5 °C obtained from OSENSA Inc.) was inserted through small holes drilled in the microwave oven and Teflon chamber. Substrates coated with the BCP film and heating element (a high resistivity silicon shard: 1.5 × 1.5 cm^2, p-type, ⟨100⟩, 525 ± 25 μm thickness, 8.4 Ω·cm) were put into a Teflon chamber and arranged as shown in Figure S3. The chamber was sealed, power level 5 selected (∼600 W), and the microwave oven turned on manually. The microwave oven was manually turned off when the desired temperature was reached. The temperature was monitored and recorded until the wafer had cooled to around 40 °C.

Metalization. For PS-*b*-P2VP films, a metalization step was employed to improve visualization by scanning electron microscopy (SEM). PS-*b*-P2VP films were immersed in an aqueous platinum salt solution (20 mM Na_2PtCl_4 and 0.250 M HCl) for 3 h. The films were then removed from solution, rinsed with ultrapure water, and dried under a nitrogen stream. The metalized PS-*b*-P2VP samples were then inserted in a Harrick plasma cleaner/sterilizer PDC-32G and treated by oxygen plasma (0.6 Torr, 45 s) to etch the polymer film and to reduce Pt^{2+} to Pt metal. For PS-*b*-PMMA samples, a brief oxygen plasma step (0.6 Torr, 15 s) was used to increase contrast under SEM (Hitachi S-4800) at 15 kV and AFM.

Conflict of Interest: The authors declare no competing financial interest.

Acknowledgment. This work was supported by NSERC, Alberta Innovates Technology Futures, and NRC-NINT. The authors thank the University of Alberta Centre for Nanofabrication (the NanoFab) for clean room support. The authors also thank Brian Olsen and Dr. Erik Luber for discussing and designing the table of contents image, and Yuyu Yao for taking photographs of the laboratory apparatus.

Supporting Information Available: More detail of setup information, AFM images, SEM images, temperature profiles, and temperature data. This material is available free of charge *via* the Internet at http://pubs.acs.org.

REFERENCES AND NOTES

1. Bates, F. S.; Fredrickson, G. H. Block Copolymers—Designer Soft Materials. *Phys. Today* **1999**, *52*, 32–38.
2. Harrison, C.; Adamson, D. H.; Cheng, Z.; Sebastian, J. M.; Sethuraman, S.; Huse, D. A.; Register, R. A.; Chaikin, P. M. Mechanisms of Ordering in Striped Patterns of Diblock Copolymers. *Science* **2000**, *290*, 1558–1561.
3. Cheng, J. Y.; Ross, C. A.; Smith, H. I.; Thomas, E. L. Templated Self-Assembly of Block Copolymers: Top-Down Helps Bottom-Up. *Adv. Mater.* **2006**, *18*, 2505–2521.
4. Bang, J.; Jeong, U.; Ryu, D. Y.; Russell, T. P.; Hawker, C. J. Block Copolymer Nanolithography: Translation of Molecular Level Control to Nanoscale Patterns. *Adv. Mater.* **2009**, *21*, 4769–4792.
5. Darling, S. B. Directing the Self-Assembly of Block Copolymers. *Prog. Polym. Sci.* **2007**, *32*, 1152–1204.
6. Bates, C. M.; Maher, M. J.; Janes, D. W.; Ellison, C. J.; Willson, C. G. Block Copolymer Lithography. *Macromolecules* **2014**, *47*, 2–12.
7. Kim, H.-C.; Park, S.-M.; Hinsberg, W. D. Block Copolymer Based Nanostructures: Materials, Processes, and Applications to Electronics. *Chem. Rev.* **2010**, *110*, 146–177.
8. Broers, A. N. Resolution Limits for Electron-Beam Llithography. *IBM J. Res. Dev.* **1988**, *32*, 502–513.
9. Ito, T.; Okazaki, S. Pushing the Limits of Lithography. *Nature* **2000**, *406*, 1027–1031.
10. Chai, J.; Buriak, J. M. Using Cylindrical Domains of Block Copolymers To Self-Assemble and Align Metallic Nanowires. *ACS Nano* **2008**, *2*, 489–501.
11. Wu, N. L. Y.; Harris, K. D.; Buriak, J. M. Conversion of Bilayers of PS-*b*-PDMS Block Copolymer into Closely Packed, Aligned Silica Nanopatterns. *ACS Nano* **2013**, *7*, 5596–5606.
12. Edwards, E. W.; Montague, M. F.; Solak, H. H.; Hawker, C. J.; Nealey, P. F. Precise Control over Molecular Dimensions of Block-Copolymer Domains Using the Interfacial Energy of Chemically Nanopatterned Substrates. *Adv. Mater.* **2004**, *16*, 1315–1319.
13. Cheng, J. Y.; Mayes, A. M.; Ross, C. A. Nanostructure Engineering by Templated Self-Assembly of Block Copolymers. *Nat. Mater.* **2004**, *3*, 823–828.
14. Ruiz, R.; Kang, H.; Detcheverry, F. A.; Dobisz, E.; Kercher, D. S.; Albrecht, T. R.; de Pablo, J. J.; Nealey, P. F. Density Multiplication and Improved Lithography by Directed Block Copolymer Assembly. *Science* **2008**, *321*, 936–939.
15. Chuang, V. P.; Gwyther, J.; Mickiewicz, R. A.; Manners, I.; Ross, C. A. Templated Self-Assembly of Square Symmetry Arrays from an ABC Triblock Terpolymer. *Nano Lett.* **2009**, *9*, 4364–4369.
16. Ferrarese, L. F.; Giammaria, T. J.; Ceresoli, M.; Seguini, G.; Sparnacci, K.; Antonioli, D.; Gianotti, V.; Laus, M.; Perego, M. Rapid Thermal Processing of Self-Assembling Block Copolymer Thin Films. *Nanotechnology* **2013**, *24*, 315601.
17. Cheng, J. Y.; Rettner, C. T.; Sanders, D. P.; Kim, H.-C.; Hinsberg, W. D. Dense Self-Assembly on Sparse Chemical Patterns: Rectifying and Multiplying Lithographic Patterns Using Block Copolymers. *Adv. Mater.* **2008**, *20*, 3155–3158.
18. Ouk Kim, S.; Solak, H. H.; Stoykovich, M. P.; Ferrier, N. J.; de Pablo, J. J.; Nealey, P. F. Epitaxial Self-Assembly of Block Copolymers on Lithographically Defined Nanopatterned Substrates. *Nature* **2003**, *424*, 411.
19. Stoykovich, M. P.; Mueller, M.; Kim, S. O.; Solak, H. H.; Edwards, E. W.; de Pablo, J. J.; Nealey, P. F. Directed Assembly of Block Copolymer Blends into Nonregular Device-Oriented Structures. *Science* **2005**, *308*, 1442–1446.
20. Stoykovich, M. P.; Kang, H.; Daoulas, K. C.; Liu, G.; Liu, C.-C.; de Pablo, J. J.; Mueller, M.; Nealey, P. F. Directed Self-Assembly of Block Copolymers for Nanolithography: Fabrication of Isolated Features and Essential Integrated Circuit Geometries. *ACS Nano* **2007**, *1*, 168–175.
21. Zhang, X.; Harris, K. D.; Wu, N. L. Y.; Murphy, J. N.; Buriak, J. M. Fast Assembly of Ordered Block Copolymer Nanostructures through Microwave Annealing. *ACS Nano* **2010**, *4*, 7021–7029.

22. Kim, S. O.; Kim, B. H.; Kim, K.; Koo, C. M.; Stoykovich, M. P.; Nealey, P. F.; Solak, H. H. Defect Structure in Thin Films of a Lamellar Block Copolymer Self-Assembled on Neutral Homogeneous and Chemically Nanopatterned Surfaces. *Macromolecules* **2006**, *39*, 5466–5470.
23. Stoykovich, M. P.; Nealey, P. F. Block Copolymers and Conventional Lithography. *Mater. Today* **2006**, *9*, 20–29.
24. Mun, B. H.; Park, W. I.; Yin, Y.; You, B. K.; Yun, J. J.; Kim, K. H.; Jung, Y. S.; Lee, K. J. Low Power Phase Change Memory *via* Block Copolymer Self-Assembly Technology. *MRS Online Proc. Libr.* **2013**, *1556*, mrss13-1556-w10-01.
25. Park, W. I.; You, B. K.; Mun, B. H.; Seo, H. K.; Lee, J. Y.; Hosaka, S.; Yin, Y.; Ross, C. A.; Lee, K. J.; Jung, Y. S. Self-Assembled Incorporation of Modulated Block Copolymer Nanostructures in Phase-Change Memory for Switching Power Reduction. *ACS Nano* **2013**, *7*, 2651–2658.
26. Milliron, D. J.; Raoux, S.; Shelby, R. M.; Jordan-Sweet, J. Solution-Phase Deposition and Nanopatterning of GeSbSe Phase-Change Materials. *Nat. Mater.* **2007**, *6*, 352–356.
27. Naito, K.; Hieda, H.; Sakurai, M.; Kamata, Y.; Asakawa, K. 2.5-in. Disk Patterned Media Prepared by an Artificially Assisted Self-Assembling Method. *IEEE Trans. Magn.* **2002**, *38*, 1949–1951.
28. Chang, L.-W.; Wong, H. S. P. Diblock Copolymer Directed Self-Assembly for CMOS Device Fabrication. *Proc. SPIE* **2006**, *6156*, 61561.
29. Shin, D. O.; Jeong, J.-R.; Han, T. H.; Koo, C. M.; Park, H.-J.; Lim, Y. T.; Kim, S. O. A Plasmonic Biosensor Array by Block Copolymer Lithography. *J. Mater. Chem.* **2010**, *20*, 7241–7247.
30. Black, C. T. Self-Aligned Self Assembly of Multi-Nanowire Silicon Field Effect Transistors. *Appl. Phys. Lett.* **2005**, *87*, 163116.
31. Hägglund, C.; Zeltzer, G.; Ruiz, R.; Thomann, I.; Lee, H.-B.-R.; Brongersma, M. L.; Bent, S. F. Self-Assembly Based Plasmonic Arrays Tuned by Atomic Layer Deposition for Extreme Visible Light Absorption. *Nano Lett.* **2013**, *13*, 3352–3357.
32. Mizuno, H.; Buriak, J. M. Catalytic Stamp Lithography for Sub-100 nm Patterning of Organic Monolayers. *J. Am. Chem. Soc.* **2008**, *130*, 17656–17657.
33. Mizuno, H.; Buriak, J. M. Nanoscale Patterning of Organic Monolayers by Catalytic Stamp Lithography: Scope and Limitations. *ACS Appl. Mater. Interfaces* **2009**, *1*, 2711–2720.
34. Mizuno, H.; Buriak, J. M. Building Upon Patterned Organic Monolayers Produced *via* Catalytic Stamp Lithography. *ACS Appl. Mater. Interfaces* **2010**, *2*, 2301–2307.
35. *International Technology Roadmap for Semiconductors*, 2011 ed.; Semiconductor Industry Association: San Jose, CA, 2011.
36. Coulon, G.; Ausserre, D.; Russell, T. P. Interference Microscopy on Thin Diblock Copolymer Films. *J. Phys. (Paris)* **1990**, *51*, 777–786.
37. Ruiz, R.; Sandstrom, R. L.; Black, C. T. Induced Orientational Order in Symmetric Diblock Copolymer Thin Films. *Adv. Mater.* **2007**, *19*, 587–591.
38. Goldacker, T.; Abetz, V.; Stadler, R.; Erukhimovich, I.; Leibler, L. Non-centrosymmetric Superlattices in Block Copolymer Blends. *Nature* **1999**, *398*, 137–139.
39. Jeong, U.; Kim, H.-C.; Rodriguez, R. L.; Tsai, I. Y.; Stafford, C. M.; Kim, J. K.; Hawker, C. J.; Russell, T. P. Asymmetric Block Copolymers with Homopolymers: Routes to Multiple Length Scale Nanostructures. *Adv. Mater.* **2002**, *14*, 274–276.
40. Jeong, U.; Ryu, D. Y.; Kim, J. K.; Kim, D. H.; Wu, X.; Russell, T. P. Precise Control of Nanopore Size in Thin Film Using Mixtures of Asymmetric Block Copolymer and Homopolymer. *Macromolecules* **2003**, *36*, 10126–10129.
41. Koneripalli, N.; Levicky, R.; Bates, F. S.; Matsen, M. W.; Satija, S. K.; Ankner, J.; Kaiser, H. Ordering in Blends of Diblock Copolymers. *Macromolecules* **1998**, *31*, 3498–3508.
42. Winey, K. I.; Thomas, E. L.; Fetters, L. J. Swelling of Lamellar Diblock Copolymer by Homopolymer: Influences of Homopolymer Concentration and Molecular Weight. *Macromolecules* **1991**, *24*, 6182–6188.
43. Ouk Kim, S.; Solak, H. H.; Stoykovich, M. P.; Ferrier, N. J.; de Pablo, J. J.; Nealey, P. F. Epitaxial Self-Assembly of Block Copolymers on Lithographically Defined Nanopatterned Substrates. *Nature* **2003**, *424*, 411–414.
44. Stoykovich, M. P.; Müller, M.; Kim, S. O.; Solak, H. H.; Edwards, E. W.; de Pablo, J. J.; Nealey, P. F. Directed Assembly of Block Copolymer Blends into Nonregular Device-Oriented Structures. *Science* **2005**, *308*, 1442–1446.
45. Bita, I.; Yang, J. K. W.; Jung, Y. S.; Ross, C. A.; Thomas, E. L.; Berggren, K. K. Graphoepitaxy of Self-Assembled Block Copolymers on Two-Dimensional Periodic Patterned Templates. *Science* **2008**, *321*, 939–943.
46. Berry, B. C.; Bosse, A. W.; Douglas, J. F.; Jones, R. L.; Karim, A. Orientational Order in Block Copolymer Films Zone Annealed below the Order−Disorder Transition Temperature. *Nano Lett.* **2007**, *7*, 2789–2794.
47. Mokarian-Tabari, P.; Collins, T. W.; Holmes, J. D.; Morris, M. A. Cyclical "Flipping" of Morphology in Block Copolymer Thin Films. *ACS Nano* **2011**, *5*, 4617–4623.
48. Wu, N. L. Y.; Zhang, X.; Murphy, J. N.; Chai, J.; Harris, K. D.; Buriak, J. M. Density Doubling of Block Copolymer Templated Features. *Nano Lett.* **2012**, *12*, 264–268.
49. Gotrik, K. W.; Hannon, A. F.; Son, J. G.; Keller, B.; Alexander-Katz, A.; Ross, C. A. Morphology Control in Block Copolymer Films Using Mixed Solvent Vapors. *ACS Nano* **2012**, *6*, 8052–8059.
50. Misner, M. J.; Skaff, H.; Emrick, T.; Russell, T. P. Directed Deposition of Nanoparticles Using Diblock Copolymer Templates. *Adv. Mater.* **2003**, *15*, 221–224.
51. Kimura, M.; Misner, M. J.; Xu, T.; Kim, S. H.; Russell, T. P. Long-Range Ordering of Diblock Copolymers Induced by Droplet Pinning. *Langmuir* **2003**, *19*, 9910–9913.
52. Fukunaga, K.; Elbs, H.; Magerle, R.; Krausch, G. Large-Scale Alignment of ABC Block Copolymer Microdomains *via* Solvent Vapor Treatment. *Macromolecules* **2000**, *33*, 947–953.
53. Tang, C.; Lennon, E. M.; Fredrickson, G. H.; Kramer, E. J.; Hawker, C. J. Evolution of Block Copolymer Lithography to Highly Ordered Square Arrays. *Science* **2008**, *322*, 429–432.
54. Jeong, J.-W.; Park, W.-I.; Kim, M.-J.; Ross, C. A.; Jung, Y.-S. Highly Tunable Self-Assembled Nanostructures from a Poly(2-vinylpyridine-*b*-dimethylsiloxane) Block Copolymer. *Nano Lett.* **2011**, *11*, 4095–4101.
55. Albert, J. N. L.; Bogart, T. D.; Lewis, R. L.; Beers, K. L.; Fasolka, M. J.; Hutchison, J. B.; Vogt, B. D.; Epps, T. H., III. Gradient Solvent Vapor Annealing of Block Copolymer Thin Films Using a Microfluidic Mixing Device. *Nano Lett.* **2011**, *11*, 1351–1357.
56. Mansky, P.; Liu, Y.; Huang, E.; Russell, T. P.; Hawker, C. Controlling Polymer−Surface Interactions with Random Copolymer Brushes. *Science* **1997**, *275*, 1458–1460.
57. Welander, A. M.; Craig, G. S. W.; Tada, Y.; Yoshida, H.; Nealey, P. F. Directed Assembly of Block Copolymers in Thin to Thick Films. *Macromolecules* **2013**, *46*, 3915–3921.
58. Skaug, M. J.; Coffey, B. M.; Schwartz, D. K. Colloidal Transfer Printing. *ACS Appl. Mater. Interfaces* **2013**, *5*, 12854–12859.
59. Kim, E.; Ahn, H.; Park, S.; Lee, H.; Lee, M.; Lee, S.; Kim, T.; Kwak, E.-A.; Lee, J. H.; Lei, X.; *et al.* Directed Assembly of High Molecular Weight Block Copolymers: Highly Ordered Line Patterns of Perpendicularly Oriented Lamellae with Large Periods. *ACS Nano* **2013**, *7*, 1952–1960.
60. *International Technology Roadmap for Semiconductors*, 2007 ed.; Semiconductor Industry Association: San Jose, CA, 2007.
61. Zhang, X.; Murphy, J. N.; Wu, N. L. Y.; Harris, K. D.; Buriak, J. M. Rapid Assembly of Nanolines with Precisely Controlled Spacing from Binary Blends of Block Copolymers. *Macromolecules* **2011**, *44*, 9752–9757.
62. Jeong, J. W.; Hur, Y. H.; Kim, H.-j.; Kim, J. M.; Park, W. I.; Kim, M. J.; Kim, B. J.; Jung, Y. S. Proximity Injection of Plasticizing Molecules to Self-Assembling Polymers for Large-Area, Ultrafast Nanopatterning in the Sub-10-nm Regime. *ACS Nano* **2013**, *7*, 6747–6757.
63. Welander, A. M.; Kang, H.; Stuen, K. O.; Solak, H. H.; Mueller, M.; de Pablo, J. J.; Nealey, P. F. Rapid Directed Assembly of

Block Copolymer Films at Elevated Temperatures. *Macromolecules* **2008**, *41*, 2759–2761.
64. Park, W. I.; Kim, K.; Jang, H.-I.; Jeong, J. W.; Kim, J. M.; Choi, J.; Park, J. H.; Jung, Y. S. Directed Self-Assembly with Sub-100 Degrees Celsius Processing Temperature, Sub-10 Nanometer Resolution, and Sub-1 Minute Assembly Time. *Small* **2012**, *8*, 3762–3768.
65. Gotrik, K. W.; Ross, C. A. Solvothermal Annealing of Block Copolymer Thin Films. *Nano Lett.* **2013**, *13*, 5117–5122.
66. Black, C. T.; Guarini, K. W.; Ruiz, R.; Sikorski, E. M.; Babich, I. V.; Sandstrom, R. L.; Zhang, Y. Polymer Self Assembly in Semiconductor Microelectronics. *IBM J. Res. Dev.* **2007**, *51*, 605–633.
67. Ko, C.-J.; Lin, Y.-K.; Chen, F.-C. Microwave Annealing of Polymer Photovoltaic Devices. *Adv. Mater.* **2007**, *19*, 3520–3523.
68. Kitchen, H. J.; Vallance, S. R.; Kennedy, J. L.; Tapia-Ruiz, N.; Carassiti, L.; Harrison, A.; Whittaker, A. G.; Drysdale, T. D.; Kingman, S. W.; Gregory, D. H. Modern Microwave Methods in Solid-State Inorganic Materials Chemistry: From Fundamentals to Manufacturing. *Chem. Rev.* **2014**, *114*, 1170–1206.
69. Kappe, C. O. Unraveling the Mysteries of Microwave Chemistry Using Silicon Carbide Reactor Technology. *Acc. Chem. Res.* **2013**, *46*, 1579–1587.
70. Clark, D. E.; Sutton, W. H. Microwave Processing of Materials. *Annu. Rev. Mater. Sci.* **1996**, *26*, 299–331.
71. Gedye, R.; Smith, F.; Westaway, K.; Ali, H.; Baldisera, L.; Laberge, L.; Rousell, J. The Use of Microwave Ovens for Rapid Organic Synthesis. *Tetrahedron Lett.* **1986**, *27*, 279–282.
72. Strauss, C. R.; Trainor, R. W. Developments in Microwave-Assisted Organic Chemistry. *Aust. J. Chem.* **1995**, *48*, 1665–1692.
73. James, R. B.; Bolton, P. R.; Alvarez, R. A.; Christie, W. H.; Valiga, R. E. Melting of Silicon Surfaces by High-Power Pulsed Microwave Radiation. *J. Appl. Phys.* **1988**, *64*, 3243–3253.
74. Zhang, X.; Murphy, J. N.; Wu, N. L. Y.; Harris, K. D.; Buriak, J. M. Rapid Assembly of Nanolines with Precisely Controlled Spacing from Binary Blends of Block Copolymers. *Macromolecules* **2011**, *44*, 9752–9757.
75. Borah, D.; Shaw, M. T.; Holmes, J. D.; Morris, M. A. Sub-10 nm Feature Size PS-*b*-PDMS Block Copolymer Structures Fabricated by a Microwave-Assisted Solvothermal Process. *ACS Appl. Mater. Interfaces* **2013**, *5*, 2004–2012.
76. Borah, D.; Senthamaraikannan, R.; Rasappa, S.; Kosmala, B.; Holmes, J. D.; Morris, M. A. Swift Nanopattern Formation of PS-*b*-PMMA and PS-*b*-PDMS Block Copolymer Films Using a Microwave Assisted Technique. *ACS Nano* **2013**, *7*, 6583–6596.
77. Zohm, H.; Kasper, E.; Mehringer, P.; Müller, G. A. Thermal Processing of Silicon Wafers with Microwave Co-Heating. *Microelectron. Eng.* **2000**, *54*, 247–253.
78. *Tables of Dielectric Materials*, Vol. IV; Lab for Insulation Research, Massachusetts Institute of Techchnology: Cambridge, MA, 1953.
79. Chai, J.; Wang, D.; Fan, X.; Buriak, J. M. Assembly of Aligned Linear Metallic Patterns on Silicon. *Nat. Nanotechnol.* **2007**, *2*, 500–506.
80. Shin, D. O.; Mun, J. H.; Hwang, G.-T.; Yoon, J. M.; Kim, J. Y.; Yun, J. M.; Yang, Y.-B.; Oh, Y.; Lee, J. Y.; Shin, J.; *et al.* Multicomponent Nanopatterns by Directed Block Copolymer Self-Assembly. *ACS Nano* **2013**, *7*, 8899–8907.
81. Park, S.-M.; Craig, G. S. W.; La, Y.-H.; Solak, H. H.; Nealey, P. F. Square Arrays of Vertical Cylinders of PS-*b*-PMMA on Chemically Nanopatterned Surfaces. *Macromolecules* **2007**, *40*, 5084–5094.